Journal of Power Sources 437 (2019) 226895

Contents lists available at ScienceDirect

Journal of Power Sources

journal homepage: www.elsevier.com/locate/jpowsour

Electrical and electrochemical properties of the Sr(Fe,Co,Mo)$O_{3-\delta}$ system as air electrode for reversible solid oxide cells

Víctor Zapata-Ramírez [a], Glenn C. Mather [a], María Teresa Azcondo [b], Ulises Amador [b], Domingo Pérez-Coll [a,*]

[a] Instituto de Cerámica y Vidrio, CSIC, Campus de Cantoblanco, 28049 Madrid, Spain
[b] Universidad San Pablo-CEU, CEU Universities, Facultad de Farmacia, Departamento de Química y Bioquímica, Urbanización Montepríncipe, Boadilla del Monte, E-28668, Madrid, Spain

HIGHLIGHTS

- Mo doping of $SrFeO_{3-\delta}$ perovskite stabilises cubic symmetry at low temperature.
- The electronic conductivity is improved on Mo and Co doping.
- Mo and Co co-doping of $SrFeO_{3-\delta}$ improves oxide-ionic conductivity.
- Excellent electrode perfomance in the IT range under anodic and cathodic bias.

ARTICLE INFO

Keywords:
Air electrode
Electrochemical performance
Ionic transport number
Ionic and electronic conductivity
Impedance spectroscopy
Reversible solid oxide cell

ABSTRACT

The effects of Co and Mo doping on the properties of $SrFeO_{3-\delta}$ perovskite as air electrode in reversible solid oxide cells have been analysed. The oxygen-ordered parent phase exhibits a high oxygen-vacancy content, which is partially reduced on doping, accompanied by stabilisation of cubic symmetry for $SrFe_{0.9}Mo_{0.1}O_{3-\delta}$ and $SrFe_{0.45}Co_{0.45}Mo_{0.1}O_{3-\delta}$ phases. All compositions lose oxygen for temperatures ≥400–450 °C, with a concomitant decrease of electron-hole conductivity. Oxide-ionic conductivity determined by Faradic efficiency significantly improves for the Co-doped composition, reaching 0.026 S cm^{-1} at 750 °C. The increase of ionic radii with reduction of Fe/Co + IV species results in greater thermal expansion for T > 450 °C. Polarization resistance without bias lowers considerably on Co doping, from ~0.55 Ω cm^2 for pure $SrFeO_{3-\delta}$, to ~0.2 Ω cm^2 for $SrFe_{0.45}Co_{0.45}Mo_{0.1}O_{3-\delta}$ at 700 °C, but not on Mo doping (~0.5 Ω cm^2). However, under cathodic and anodic polarization, a comparable, excellent performance at 650 °C of all compositions indicates their considerable promise as air electrodes for reversible solid oxide fuel cell-electrolyser systems, particularly for $SrFe_{0.9}Mo_{0.1}O_{3-\delta}$ with more moderate thermal expansion.

1. Introduction

The drive towards achieving a fully sustainable energy sector is largely propelled by global alarm over the adverse and potentially catastrophic effects of increasing CO_2 emissions, the need to decrease energy dependence on volatile states with undemocratic regimes and the anticipated peak and decline of worldwide oil supply. Hydrogen is a highly promising component of a sustainable energy portfolio for both stationary and transport power applications due to is ready transportation and facile oxidation to water [1]. The conversion of hydrogen and low hydrocarbons can occur with high efficiency in a solid oxide fuel cell, made up of a ceramic electrolyte, porous ceramic cathode and porous cermet anode. With the use of waste heat in combined heat and power (CHP) applications, unrivalled efficiencies of up to 85% may be achieved [2]. Operation of the ceramic cells in reverse mode (solid oxide electrolyser cells, SOECs) achieves high temperature electrolysis requiring less electrical energy and higher electrolytic efficiency than low-temperature analogues [3,4]. Electrical energy may be both supplied and extracted in a single cell giving rise to the concept of reversible or regenerative solid oxide cells. The energy provided from intermittent and discontinuous renewable energy supplies, such as solar or wind, coupled with waste heat from industrial or other sources may provide

* Corresponding author.
E-mail address: dpcoll@icv.csic.es (D. Pérez-Coll).

https://doi.org/10.1016/j.jpowsour.2019.226895
Received 22 May 2019; Received in revised form 11 July 2019; Accepted 15 July 2019
Available online 17 July 2019
0378-7753/

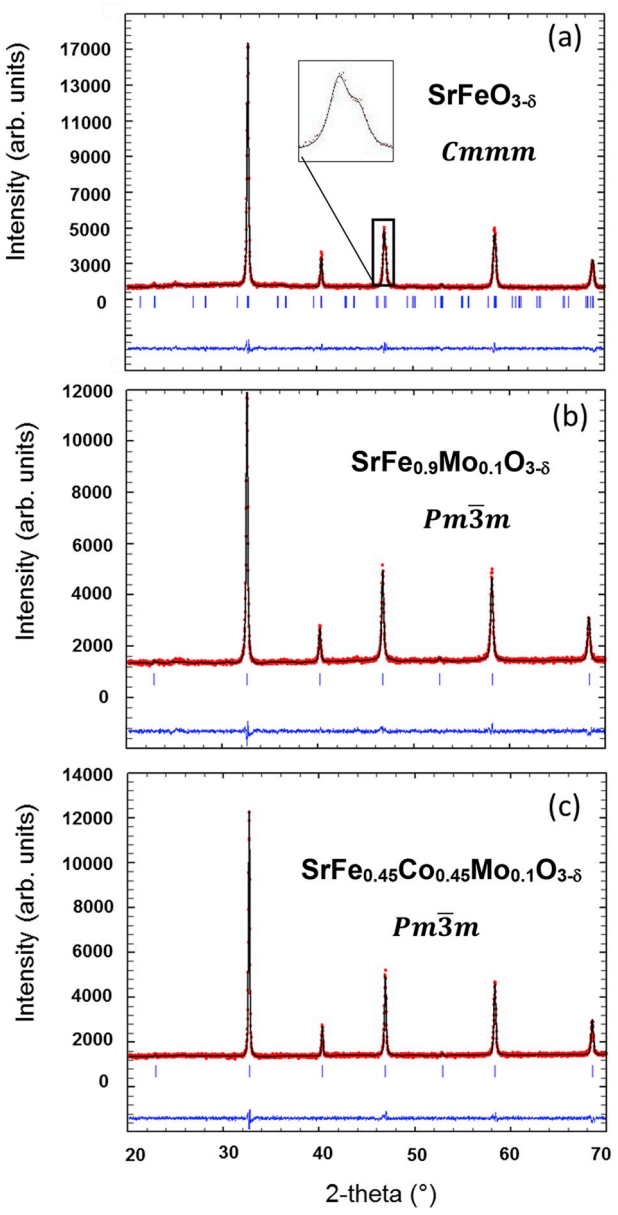

Fig. 1. Experimental (red circles), calculated (continuous black line) and difference (continuous blue line at bottom of each panel) X-ray diffraction patterns of (a) $SrFeO_{3-\delta}$, (b) $SrFe_{0.9}Mo_{0.1}O_{3-\delta}$ and (c) $SrFe_{0.45}Co_{0.45}Mo_{0.1}O_{3-\delta}$. The position of Bragg peaks is indicated by vertical bars; peak splitting in the $SrFeO_{3-\delta}$ phase is shown in the inset of (a). (For interpretation of the references to colour in this figure legend, the reader is referred to the Web version of this article.)

energy for steam electrolysis. The stored hydrogen can then be converted to electrical energy via reoxidation to water when power from renewable sources is not available.

There is much focus on achieving good performance in both fuel-cell and electrolyser modes in an intermediate temperature range (500–800 °C) since the traditionally high operating temperatures (~1000 °C) lead to degradation of materials, lower lifetimes, and increase the start-up and shutdown times, limiting their possible applications. An operation temperature below 600 °C has the further advantage that cheaper balance-of-plant materials such as stainless steel may be employed.

Materials commonly used as air electrodes in SOFCs such as perovskites based on lanthanum manganite ($LaMnO_{3-\delta}$) and lanthanum cobaltite ($LaCoO_{3-\delta}$) may not be suitable in electrolysis cells (anodic polarization) since high local oxygen partial pressures can lower the

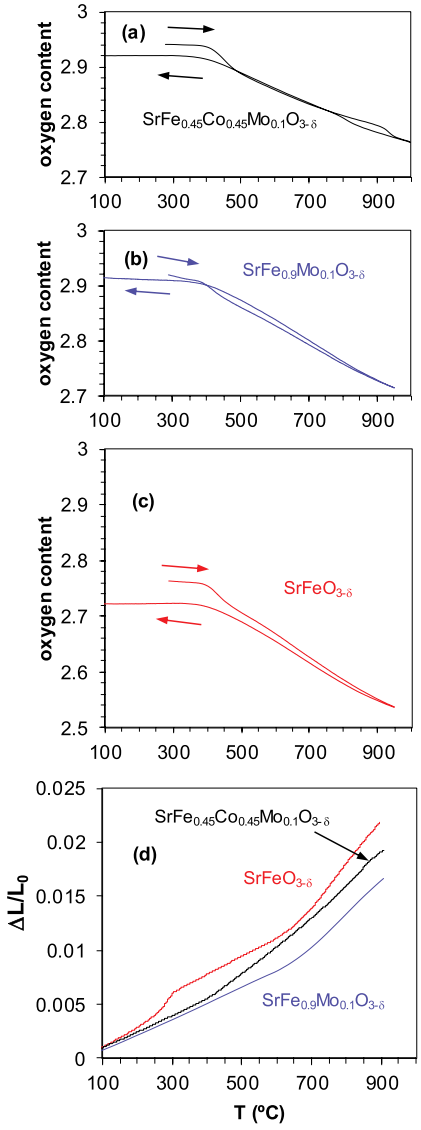

Fig. 2. Oxygen content as a function of temperature, determined by titration and thermogravimetry in air (a), (b) and (c), and relative linear thermal expansion as a function of temperature of densified samples (d) of $SrFeO_{3-\delta}$, $SrFe_{0.9}Mo_{0.1}O_{3-\delta}$ and $SrFe_{0.45}Co_{0.45}Mo_{0.1}O_{3-\delta}$.

Table 1
Room temperature average oxidation state (A.O.S) of Fe and (Fe,Co) cations determined by titration, and corresponding stoichiometric contents of Fe^{3+}, Fe^{4+}, $(Fe,Co)^{3+}$, $(Fe,Co)^{4+}$ and O^{2-} determined by electroneutrality (oxidation state of molybdenum is assumed to be +6).

Composition	A.O.S	$[Fe^{3+}]$	$[Fe^{4+}]$	$[Mo^{6+}]$	$[(Fe,Co)^{3+}]$	$[(Fe,Co)^{4+}]$	$[O^{2-}]$
$SrFeO_{3-\delta}$	Fe: 3.52	0.47	0.53				2.76
$SrFe_{0.9}Mo_{0.1}O_{3-\delta}$	Fe: 3.60	0.37	0.53	0.1			2.92
$SrFe_{0.45}Co_{0.45}Mo_{0.1}O_{3-\delta}$	(Fe,Co): 3.64			0.1	0.32	0.58	2.94

Table 2
Thermal expansion coefficients (TEC) for different compositions sintered at 1200-1250 °C.

Composition	TEC x 10^{-6} (K^{-1})
$SrFeO_{3-\delta}$	17.7 (RT-250 °C)
	17.2 (350–650 °C)
	40.4 (650–900 °C)
$SrFe_{0.9}Mo_{0.1}O_{3-\delta}$	14.6 (RT-650 °C)
	30.8 (650–900 °C)
$SrFe_{0.45}Co_{0.45}Mo_{0.1}O_{3-\delta}$	14.8 (RT-400 °C)
	24.5 (400–650 °C)
	30.8 (650–900 °C)

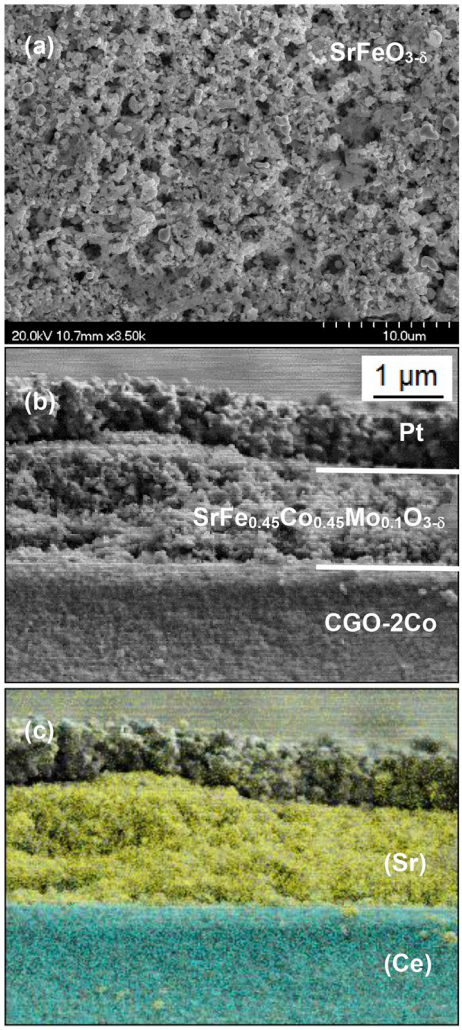

Fig. 3. SEM images of a top view of $SrFeO_{3-\delta}$ deposited over CGO-2Co electrolyte (a), a cross section view of a semi-cell employed in electrochemical characterisation based on Pt/$SrFe_{0.45}Co_{0.45}O_{3-\delta}$/CGO-2Co (b), and EDXS mapping of the half-cell corresponding to Sr and Ce species (c).

local oxygen-vacancy concentration and, in turn, performance [5,6]. However, more recent investigations reveal that other perovskites such as $SrCo_{1-x}Mo_xO_{3-\delta}$ exhibit high efficiency as air electrode in both electrolysis and fuel-cell modes on employing a ceria-based electrolyte [7], but with better performance on electrolysis. This dichotomy between

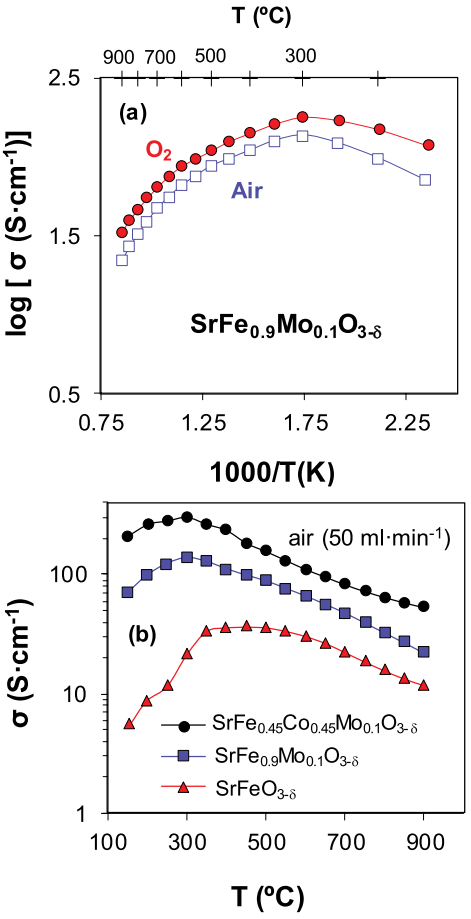

Fig. 4. (a) Arrhenius representation of total conductivity in air (squares) and O_2 (circles) atmospheres for $SrFe_{0.9}Mo_{0.1}O_{3-\delta}$ and (b) comparison of electrical conductivity as a function of temperature of $SrFeO_{3-\delta}$ (triangles), $SrFe_{0.9}Mo_{0.1}O_{3-\delta}$ (squares) and $SrFe_{0.45}Co_{0.45}Mo_{0.1}O_{3-\delta}$ (circles) under an air flux of 50 ml/min.

performances of ostensibly similar systems for reduction and oxidation reactions in fuel cells and electrolysers indicates that compositional factors may be critical to many currently unknown aspects of the electrochemical process.

The exceptional mixed-conducting properties of $SrCoO_{3-\delta}$-based materials provide excellent permeation [8]. However, sensitivity to carbonation in the presence of CO_2 and high thermal expansion coefficients are problems for practical application as SOFC cathode. In addition, a number of phase transitions are encountered on heating related to ordering and disordering of oxygen vacancies [9].

Similar perovskite compositions based on $SrFeO_{3-\delta}$ have been gaining attention both as the positive and negative electrodes of symmetrical SOFCs [10–12]. The symmetrical configuration provides a solution to sulphur poisoning or coke formation on the anode during operation with hydrocarbons as fuel since the malignant species may be removed on flushing with air on reverse operation. $SrFeO_{3-\delta}$-based compositions show good mixed conductivity but, as is the case for $SrCoO_{3-\delta}$, the tendency for vacancy ordering accompanied by a phase change to brownmillerite limits oxygen transport with decreasing pO_2 [13,14].

Doping strategies have been employed in both these systems involving replacement of Fe or Co with higher valence cations to limit oxygen loss and associated phase transitions, as well as mitigating the effects of high thermal expansion and carbonation [11,12,15,16]. Molybdenum is a good candidate for this role since the facility for presenting mixed oxidation states provides good electrocatalytic activity and electronic properties [7,10,17,18]. Moreover, the ability to adopt

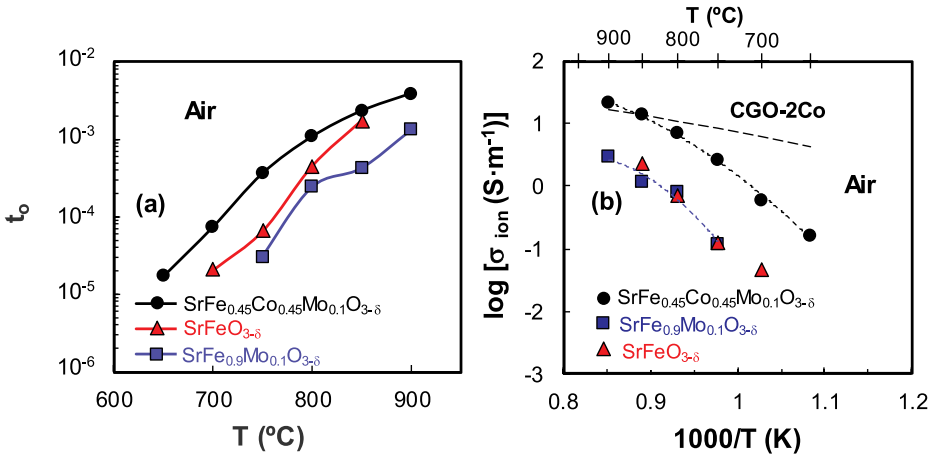

Fig. 5. Temperature dependence of the ionic transport number (a) and Arrhenius representation of ionic conductivity, of $SrFeO_{3-\delta}$ (triangles), $SrFe_{0.9}Mo_{0.1}O_{3-\delta}$ (squares) and $SrFe_{0.45}Co_{0.45}Mo_{0.1}O_{3-\delta}$ (circles). The ionic conductivity of $Ce_{0.9}Gd_{0.1}O_{2-\delta}$ + 2 mol% Co (CGO-2Co) is also represented in (b) for comparison.

different coordination environments allows for a range of oxygen stoichiometries.

Here, we explore the effects of Mo doping in $SrFeO_{3-\delta}$ and a mixed Fe/Co perovskite composition ($SrFe_{0.45}Co_{0.45}Mo_{0.1}O_{3-\delta}$) on the electrical conductivity and electrochemical characteristics under both anodic and cathodic polarization with a view to exploiting their potential for application in reversible solid oxide cells. Electronic and ionic transport properties were specifically determined and related to the electrochemical behaviour.

2. Experimental

2.1. Synthesis, structural and microstructural characterisation

Compositions of $SrFeO_{3-\delta}$ (SF), $SrFe_{0.9}Mo_{0.1}O_{3-\delta}$ (SFM) and $SrFe_{0.45}Co_{0.45}Mo_{0.1}O_{3-\delta}$ (SFCM) were prepared by a citrate-nitrate process based on the Pechini method [19]. Stoichiometric contents of $Sr(NO_3)_2$, $Fe(NO_3)_3{\cdot}xH_2O$, $Co(NO_3)_2{\cdot}xH_2O$ and $(NH_4)_6Mo_7O_{24}{\cdot}xH_2O$ were dissolved in distilled water with continuous stirring on a hotplate at 50 °C. Subsequently, citric acid, in a molar ratio of 10:1 with respect to the final product, and ethylene glycol, in a molar ratio of 40:1, were added while temperature was increased to 60–80 °C for 2 h and then to >90 °C for 4 h and overnight at > 100 °C. This produced a dark-brown polymerised complex which was heated at 350 °C for 4 h to achieve pyrolysis, then at 600 °C for 4 h to remove any residual organic component. The resultant fine powder was ground in a mortar and pestle and subsequently heated at 1000 °C for 4 h followed by attrition milling at 400 rpm for 2 h in a Fritsch pulverisette planetary ball mill.

Structural characterisation of the compounds was performed by X-ray diffraction (XRD) using a Bruker D8 high-resolution diffractometer with a germanium monochromator providing monochromatic Cu $K\alpha_1$ radiation ($\lambda = 1.5406$ Å). Rietveld refinements were performed with the Fullprof program [20] on diffraction data collected in the range $20° \leq 2\theta \leq 70°$ employing a stepwidth of 0.02 and a step counting time of 2 s.

Microstructure and morphology of the samples were studied by scanning electron microscopy (SEM) using a FE-SEM Hitachi 4700 S coupled with Energy-dispersive X-ray spectroscopy (EDS-Noran).

2.2. Oxygen content, oxidation states and thermal analysis

The iron oxidation state of the as-prepared $SrFeO_{3-\delta}$ and $SrFe_{0.9}Mo_{0.1}O_{3-\delta}$ phases, the mixture of iron and cobalt oxidation state of $SrFe_{0.45}Co_{0.45}Mo_{0.1}O_{3-\delta}$ and the oxygen content (assuming charge neutrality) of all compositions were determined by redox titration as described earlier [21].

Thermogravimetric analysis (TGA) was employed to study the effect of temperature on the oxygen content using a Netzsch STA-409 PC-Luxx apparatus working in air in the range 25–1000 °C with heating/cooling rates of 5 °C/min.

Dilatometry was performed on rectangular bars with approximate dimensions of 11 × 4 × 4 mm^3, previously sintered at 1200–1250 °C for 6 h, using an Adamel Lhomargy DI-24 thermomechanical equipment in the temperature range 25–900 °C with a heating ramp rate of 5 °C/min.

2.3. Total and partial components of conductivity

Total conductivity was determined by a four-probe direct current (d.c.) current-voltage measurement. Rectangular bars were prepared by pressing the powders and sintering at 1200 °C for 6 h. One pair of Pt-wire electrodes was attached to the external Pt-covered surfaces to produce a direct current flux through the length of the bars in galvanostatic mode. Another pair of Pt wires was internally located on the bars to determine the voltage difference arising between parallel planes. A potentiostat/galvanostat (Autolab PGSTAT302 N) was employed to register the current-voltage curves in galvanostatic mode between 0 and 0.1 A in steps of 0.01 A. Electrical conductivity was determined in the temperature interval 150–900 °C under atmospheres of O_2 and air on cooling at 5 °C/min in steps of 50 °C. Equilibrium was assured by maintaining the samples under the corresponding atmospheres at 900 °C for 5 h before the electrical procedure.

Oxide-ionic conductivity was determined by combination of the results of total electrical conductivity and ionic transport number, determined by Faradic Efficiency following the methodology reported elsewhere [22]. Highly densified cylindrical pellets prepared by sintering the powders at 1250–1300 °C for 6 h were attached to Pt wires by means of circular Pt electrodes on both surfaces and hermetically sealed to a home-made electrochemical cell. The cell comprises an oxygen electrochemical pump and a pO_2 sensor, based on YSZ components. The oxygen is pumped into the cell by a d.c. source connected to the sample with the external electrode in cathodic polarization. The oxygen is pumped out through the YSZ pellet using another independent d.c. source with the internal electrode cathodically polarized. On reaching the steady-state situation, in which the oxygen flux through the mixed-conducting sample corresponds to the oxygen flux through the YSZ, the relation between electrical currents is expressed as [22]:

$$t_O = \frac{I_{out}}{I_{in}} \quad (1)$$

where t_O is the oxide ionic transport number and I_{out} and I_{in} correspond to the electrical current through the YSZ and the mixed-conducting

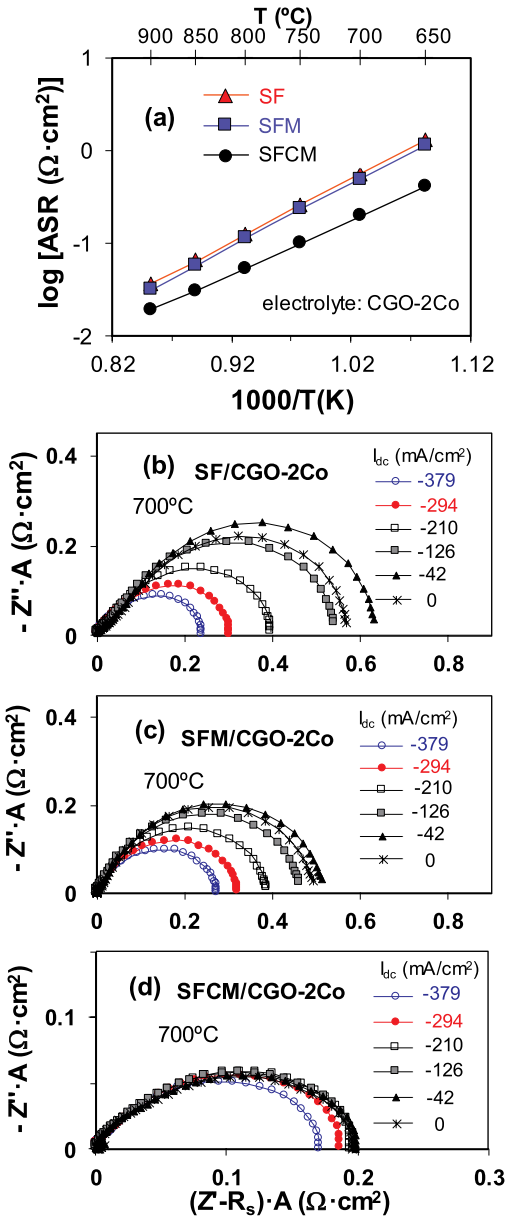

Fig. 6. Arrhenius representation of area-specific resistance of the oxygen electrochemical process for the three studied samples without dc bias (a), and impedance spectra obtained at 700 °C under different dc cathodic currents for $SrFeO_{3-\delta}$ (b), $SrFe_{0.9}Mo_{0.1}O_{3-\delta}$ (c) and $SrFe_{0.45}Co_{0.45}Mo_{0.1}O_{3-\delta}$ (d). Note that the spectra represented in b-d are displaced to the origin of the x axes for a clearer comparison of the electrode-electrolyte electrochemical process.

sample, respectively. The experiments were performed on maintaining the atmospheric $pO_2 \approx 0.21$ atm in the feed and the inner sides of the cell, such that the voltage difference in the YSZ pO_2 sensor was $E_0 = 0$, in the range 650–900 °C. The ionic conductivity was determined from the results of total conductivity and ionic transport number, according to:

$$\sigma_O = \sigma_{tot} t_O \quad (2)$$

2.4. Electrochemical analysis

The electrochemical properties of the $Sr(Fe,Co,Mo)O_{3-\delta}$ system as air electrode with ceria-based electrolytes were studied by impedance spectroscopy in air in the temperature range 650–900 °C. For this purpose, electrolyte materials were prepared by pressing powders of $Ce_{0.9}Gd_{0.1}O_{2-\delta}$ (CGO, Rhodia) in cylindrical pellets of 20 mm in diameter followed by sintering at 1500 °C for 6 h. Modified electrolytes were prepared by addition of 2 mol% Co to the CGO powders (CGO-2Co) following the methodology reported elsewhere [23]. Highly densified CGO-2Co electrolytes were obtained after sintering similarly prepared cylindrical pellets at 1100 °C for 6 h. Electrode materials were mixed with a binder (Decoflux™, WB41, Zschimmer and Schwartz), deposited on opposite faces of CGO and CGO-2Co electrolytes and sintered at 1000 °C for 1 h. Impedance spectroscopy was performed using a 3-probe configuration with circular working and counter electrodes of 5.5 mm in diameter and an external Pt ring located around the working electrode, acting as a reference electrode [24]. Impedance spectroscopy was conducted with an Autolab PGSTAT302 N instrument with a FRA2 module, applying a signal amplitude of 50 mV in the frequency range 0.1–10^6 Hz.

The effect of current on the electrode performance was analysed by imposing a d.c. bias during the impedance measurements in air. Values of direct currents were varied in the range ~ 0–400 mA·cm^{-2} in both directions of cathodic and anodic polarization in order to analyse the performance of the air electrode as cathode in fuel-cell mode and anode in electrolyser mode, respectively.

3. Results

3.1. Structural characterisation, stoichiometry, thermal behaviour and microstructural analysis

The X-ray powder diffraction patterns of the three studied phases indicated phase-pure material with the perovskite structure. $SrFe_{0.9}Mo_{0.1}O_{3-\delta}$ and $SrFe_{0.45}Co_{0.45}Mo_{0.1}O_{3-\delta}$ were cubic at the resolution of XRD and were refined accordingly in space group $Pm\bar{3}m$, giving lattice parameters of a = 3.8818(2) and 3.8692(2) Å, respectively. The XRD pattern of the $SrFeO_{3-\delta}$ phase, however, indicated greater structural complexity with readily observed peak splitting indicating lower symmetry than the simple cubic structure. A neutron powder diffraction study by Hodges et al. [13] indicated that in the $SrFeO_x$ system of composition range $2.5 \leq x \leq 3.0$ with brownmillerite ($Sr_2Fe_2O_5$, *Icmm*) and cubic ($SrFeO_3$, $Pm\bar{3}m$) end members, the varying oxygen content gives rise to two further distinct structures with ordered oxygen vacancies: $Sr_4Fe_4O_{11}$ (orthorhombic, *Cmmm*) and $Sr_8Fe_8O_{23}$ (tetragonal, *I4/mcm*). Refinement of the $SrFeO_{3-\delta}$ phase with fixed thermal vibration parameters indicated a slightly better fit with the orthorhombic model ($\chi^2 = 1.33$; $R_B = 1.61$) compared with tetragonal symmetry ($\chi^2 = 1.42$; $R_B = 1.88$), with final lattice parameters a = 10.9405(8), b = 7.6975(5) and c = 5.4581(4) Å. Similar symmetry and lattice parameters were previously reported for the same composition [12]. Nevertheless, the symmetry is highly dependent on oxygen content and thermal history with the resolution of XRD likely to provide only an indication of the correct space group. The observed and calculated XRD patterns and their difference for the three compositions are shown in Fig. 1, with peak splitting of the $SrFeO_{3-\delta}$ phase shown in the inset of Fig. 1a.

The average oxidation state, determined by redox titration, and oxygen content, assuming electroneutrality with molybdenum in a 6 + oxidation state, are presented in Table 1. The low oxygen content per formula unit of 2.76 determined for undoped $SrFeO_{3-\delta}$, corresponds to an average oxidation state of 3.52 for Fe, and is likely to be responsible for the lowering of symmetry to orthorhombic, as determined by the Rietveld refinement of XRD patterns at room temperature. The presence of Mo in the solid solution $SrFe_{0.9}Mo_{0.1}O_{3-\delta}$ produces an increase in both the oxygen content (to 2.92 per formula unit) and symmetry. The average oxidation state of Fe increases slightly to 3.60, such that the Fe^{3+} content per formula decreases from 0.47 (for undoped $SrFeO_{3-\delta}$) to 0.37 (for $SrFe_{0.9}Mo_{0.1}O_{3-\delta}$), whereas the Fe^{4+} content per formula remains practically identical (Table 1).

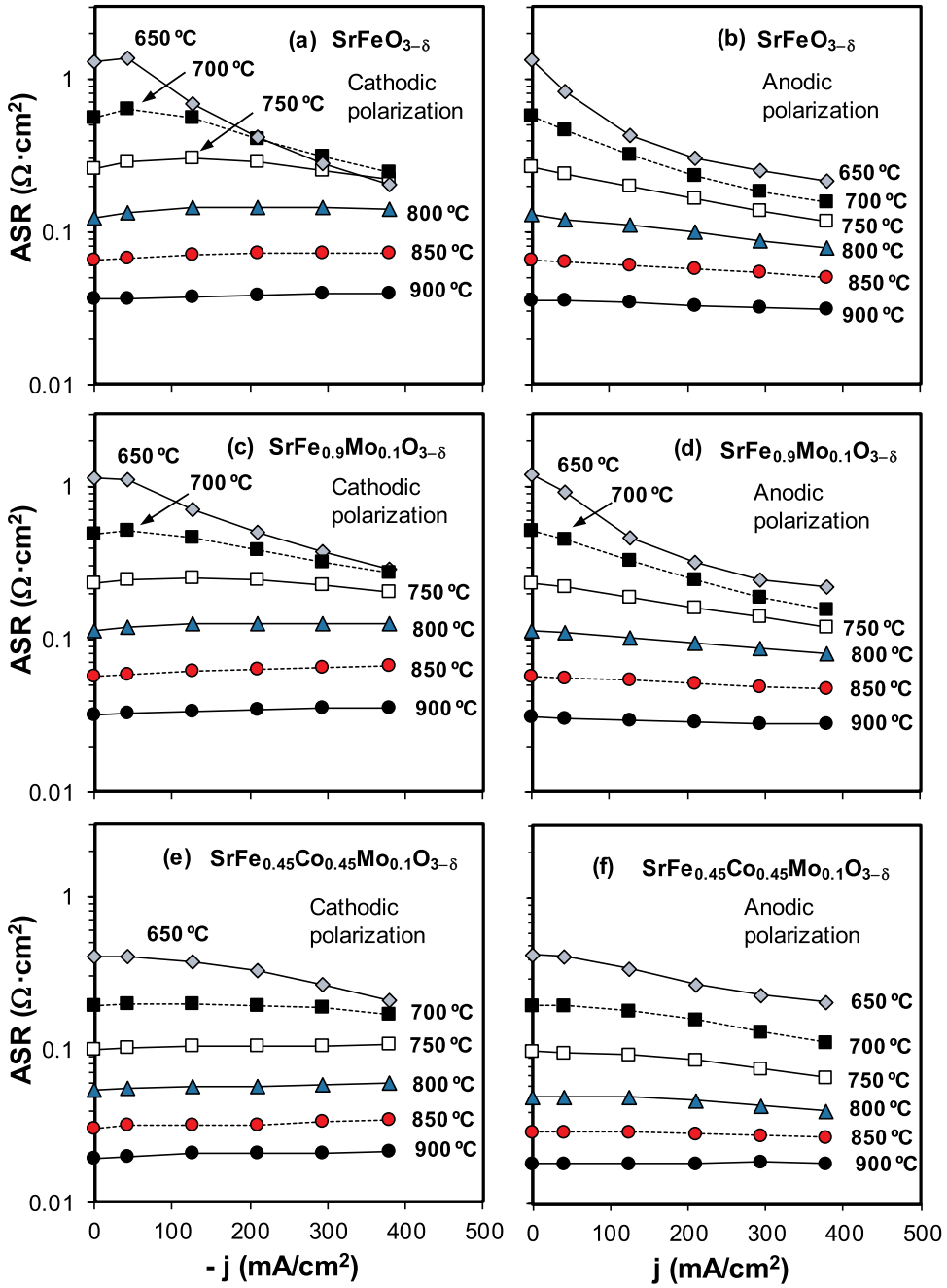

Fig. 7. Effect of dc current on the area-specific resistance of the oxygen electrochemical process in cathodic polarization (a,c,e) and anodic polarization (b,d,f) for $SrFeO_{3-\delta}$ (a,b), $SrFe_{0.9}Mo_{0.1}O_{3-\delta}$ (c,d) and $SrFe_{0.45}Co_{0.45}Mo_{0.1}O_{3-\delta}$ (e,f).

These results suggest that the incorporation of Mo^{6+} in the $SrFeO_{3-\delta}$ lattice is electrically balanced by the preferential substitution of Fe^{3+} and the incorporation of oxygen (Table 1).

Substitution of Fe for Co in the solid solution $SrFe_{0.45}Co_{0.45}Mo_{0.1}O_{3-\delta}$ leads to a slight increase of both the oxygen content and the (Fe,Co) average oxidation state to 2.94 and 3.64, respectively (Table 1). Co thus promotes an increment of the oxygen content, directly related to the oxidation states of the (Fe,Co) species, increasing the content of 4 + cations from 0.53 in $SrFe_{0.9}Mo_{0.1}O_{3-\delta}$, to 0.58 in $SrFe_{0.45}Co_{0.45}Mo_{0.1}O_{3-\delta}$.

The oxygen nonstoichiometry of the three phases determined by thermogravimetry as a function of temperature, taking into account the oxygen content at room temperature, is presented in Fig. 2a–c. All samples present an initial mass loss between 100 and 300 °C of about ~0.1–0.3% (not shown in the graph) corresponding to the loss of adsorbed water. As temperature rises, an abrupt mass loss occurs at ~450 °C corresponding to loss of oxygen and the concomitant reduction of Fe and Co cations. Relative linear thermal expansion of the sintered samples is presented in Fig. 2d in the range 100–900 °C. For $SrFeO_{3-\delta}$, an abrupt increase in the relative linear expansion is observed at ~250–300 °C with rising temperature, producing a shoulder. Very similar behaviour was previously reported [17] and attributed to a phase transition. All compositions exhibit an increase of the slope in the high-temperature range, typical of Co- and Fe-based perovskites [7,17,25], which is associated to oxygen release and the corresponding reduction of B-site cations to larger species, increasing the thermal expansion coefficient (TEC) (Table 2). Interestingly, the introduction of Mo in the $SrFeO_{3-\delta}$ network decreases the linear thermal expansion, in

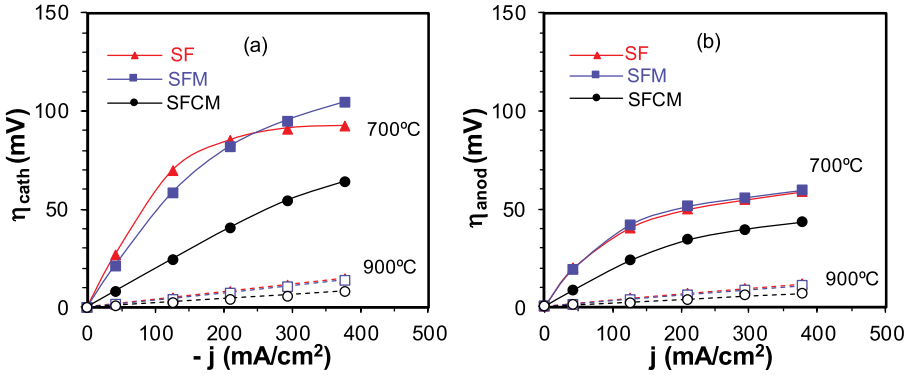

Fig. 8. Effect of current density and direction on the overpotential at the working electrode for the title compositions. Negative (a) and positive (b) currents correspond to cathodic and anodic polarization of the working electrode, respectively.

good agreement with previous results [17], due to the lower content of the larger 3 + ions, which are mainly substituted by Mo^{6+}. Moreover, the stronger Mo–O bond in comparison to that of Fe–O is expected to lower thermal expansion. On the other hand, for the Co-containing composition, $SrFe_{0.45}Co_{0.45}Mo_{0.1}O_{3-\delta}$, the transition from the lower to higher TEC regime occurs at a lower temperature compared to $SrFe_{0.9}Mo_{0.1}O_{3-\delta}$. Partial substitution of Fe for Co is expected to facilitate reduction to 3 + and 2 + cation species, due to the weaker Co–O bond in comparison to Fe–O bond, thus increasing the thermal expansion in the intermediate temperature range (~400–650 °C).

SEM images of electrode materials deposited on CGO-2Co electrolyte are shown in Fig. 3. The top view of $SrFeO_{3-\delta}$ (Fig. 3a) reveals high porosity and homogeneity of the material after deposition and sintering at 1000 °C, favouring diffusion of oxygen to the electrochemically active sites. Good adhesion between air electrode and electrolyte was observed, as shown in the cross-sectional view of $SrFe_{0.45}Co_{0.45}Mo_{0.1}O_{3-\delta}$ deposited on CGO-2Co, Fig. 3b. Moreover, the Pt-current collector, air electrode and electrolyte layers are well defined, as confirmed by EDXS analysis shown in Fig. 3c, indicating that they are chemically compatible with insignificant interdiffusion of species occurring between layers.

3.2. Electronic and ionic conductivity

The temperature dependence of total conductivity of $SrFe_{0.9}Mo_{0.1}O_{3-\delta}$ in air and O_2 atmospheres is shown in Fig. 4a; analogous results were obtained for the three different compositions. An enhancement of conductivity is observed in the more oxidising atmosphere, confirming the predominant p-type electronic character of transport associated to the creation of electron holes according to:

$$\frac{1}{2}O_2 + v_O^{\cdot\cdot} \leftrightarrow O_O^X + 2h^{\cdot} \quad (3)$$

Fig. 4a shows an increase of conductivity with temperature between 150 and 300 °C, with activation energies as low as 0.14 and 0.1 eV, for air and oxygen, respectively; for higher temperatures, conductivity decreases.

The effect of temperature on conductivity in air for the title phases is shown in Fig. 4b, where maxima between 300 and 400 °C occur due to a pronounced decrease of conductivity for higher temperatures. This drop correlates well with the sudden decrease of oxygen content determined by TG measurements in the same temperature range (Fig. 2a–c), indicating that it is attributable to the creation of oxygen vacancies and the elimination of electron holes as temperature rises. The introduction of Mo in the $SrFe_{0.9}Mo_{0.1}O_{3-\delta}$ network increases the electronic conductivity several times in comparison to the undoped composition. Moreover, the simultaneous introduction of Mo and Co in the Fe position ($SrFe_{0.45}Co_{0.45}Mo_{0.1}O_{3-\delta}$) enhances the conductivity by a factor of 3 at low temperature with respect to $SrFe_{0.9}Mo_{0.1}O_{3-\delta}$. The maximum values of conductivity are 36, 136 and 298 Scm^{-1} for $SrFeO_{3-\delta}$, $SrFe_{0.9}Mo_{0.1}O_{3-\delta}$ and $SrFe_{0.45}Co_{0.45}Mo_{0.1}O_{3-\delta}$, respectively. The lower conductivity obtained for the undoped $SrFeO_{3-\delta}$ phase is mainly associated with the low oxygen content, as determined from the titration and TG measurements (Fig. 2), and the greater tendency for vacancy ordering which is manifested at room temperature by adoption of lower symmetry. From the analysis of the oxidation states of the Fe–Co cations (Table 1), it follows that the Fe^{4+} content remained practically constant on introduction of Mo in the Fe position, resulting in a similar concentration of electron holes. However, the higher oxygen content favours higher symmetry and also conduction channels along the Fe^{4+}–O^{2-}–Fe^{3+} [17,26] network, leading to greater electronic conductivity in $SrFe_{0.9}Mo_{0.1}O_{3-\delta}$ compared to $SrFeO_{3-\delta}$. It is expected that if the Mo content increases beyond a certain point, these chains would be disrupted, leading to lower electronic conductivity [26]. The simultaneous presence of Co and Mo on the B sites in $SrFe_{0.45}Co_{0.45}Mo_{0.1}O_{3-\delta}$, brings about an increase of the oxygen content and concentration of 4 + Fe/Co species (Table 1). The corresponding increase in electron-hole concentration and the lower bond strength of Co–O in comparison to Fe–O are both likely to be responsible for the considerable enhancement of electronic conductivity [27]. As temperature rises, some oxygen disordering is expected in $SrFeO_{3-\delta}$, which contributes to decreasing the differences in conductivity between the samples above 600 °C, Fig. 4b.

Ionic transport numbers for the different compositions determined by Faradic Efficiency under air are shown in Fig. 5a. It is expected that the total conductivity is essentially electronic under oxidising conditions; hence, the oxide-ionic contribution to the electrical transport is several orders of magnitude lower than the electronic contribution in the intermediate temperature range. Notably, the oxide-ionic component increases progressively as temperature rises, leading to values of $t_O > 10^{-3}$ at 900 °C. The main reason for this is the loss of oxygen and the concomitant increment of oxygen vacancies and decrease of electron holes (eq. (3) goes to the left). Nevertheless, distinct ionic transport properties are observed for the three compositions, as shown from their Arrhenius dependence of ionic conductivity in air, Fig. 5b. It is apparent that $SrFe_{0.45}Co_{0.45}Mo_{0.1}O_{3-\delta}$ presents values of ionic conductivity in the high temperature range (800–900 °C) which are comparable to those of the CGO-2Co electrolyte (indicated in the figure).

However, as temperature decreases, the ionic conductivity of the electrode material decreases at a greater rate than the CGO-2Co electrolyte. On cooling, the increasing oxygen content and decreasing oxygen-vacancy concentration (Fig. 2a), leads to a difference in conductivity between the two compositions of about one order of magnitude at 700 °C. In contrast, $SrFeO_{3-\delta}$ and $SrFe_{0.9}Mo_{0.1}O_{3-\delta}$ exhibit similar ionic conductivities, approximately an order of magnitude lower than the $SrFe_{0.45}Co_{0.45}Mo_{0.1}O_{3-\delta}$ composition. As is the case with electronic conductivity, doping with cobalt also improves the mobility of the oxygen vacancies due to the lower strength of the Co–O bond in

comparison to Fe–O. Such a result is consistent with the expectation that the oxygen migration barrier lowers as the strength of oxygen-cation bonds decreases [28], leading to a higher oxide-ionic conductivity.

3.3. Electrochemical properties

The electrochemical performance of the electrode materials deposited on CGO-2Co electrolytes was analysed by impedance spectroscopy in 3-probe electrochemical cells with a reference electrode [24]. Fig. 6a shows the Arrhenius representation of the area-specific resistance (ASR) of the electrode-electrolyte electrochemical process without application of dc bias for the three electrode compositions. It is observed that $SrFeO_{3-\delta}$ and $SrFe_{0.9}Mo_{0.1}O_{3-\delta}$ present very similar values, with an activation energy of 1.34 eV, whereas the dual presence of Mo and Co, in $SrFe_{0.45}Co_{0.45}Mo_{0.1}O_{3-\delta}$, enhances the electrochemical performance considerably, decreasing the activation energy to 1.15 eV. The overall oxygen electrochemical reaction in mixed conducting electrodes involves reaction at the surface, oxygen incorporation into the network and corresponding diffusion through the bulk [29]. The transformation of oxygen to oxide ions and incorporation into the lattice involves electron- and ion-transfer steps, whereas chemical diffusion includes the transport of ionic and electronic defects. Electron-hole conductivity, Fig. 4b, was clearly lower for $SrFeO_{3-\delta}$ compared to that observed for Mo and Mo/Co doped compositions; this difference is mainly attributable to oxygen ordering in $SrFeO_{3-\delta}$, especially at lower temperature, and low oxygen content, as mentioned above. On the other hand, Fig. 5 revealed that $SrFeO_{3-\delta}$ and $SrFe_{0.9}Mo_{0.1}O_{3-\delta}$ present similar ionic conductivities, whereas that of $SrFe_{0.45}Co_{0.45}Mo_{0.1}O_{3-\delta}$ is considerably greater. Although apparent differences in electronic conductivity are observed in the intermediate-high temperature range, the bulk transport path of oxygen ions seems to be determinant for the overall electrochemical process, as discussed below.

Fig. 6 b-d show typical impedance spectra for the series as a function of dc cathodic bias at 700 °C. It is apparent that the magnitude of the cathodic current density has a determining influence on the electrode-polarization resistance, although the different compositions are affected to different degrees according to their catalytic and mixed-transport properties. Interestingly, the cathode performance is much more influenced by dc bias in the lower temperature range than at higher temperature (Fig. 7 a, c and e). Moreover, the temperature interval which is affected depends on composition. For $SrFeO_{3-\delta}$ and $SrFe_{0.9}Mo_{0.1}O_{3-\delta}$, the cathodic performance is practically independent of current between 750 and 900 °C, whereas a monotonous decrease of ASR is apparent at 650–700 °C for current densities higher than ~50 $mA{\cdot}cm^{-2}$, Fig. 7 a, c.

The ASR of $SrFe_{0.45}Co_{0.45}Mo_{0.1}O_{3-\delta}$ is essentially current independent between 700 and 900 °C, showing a progressive decrease for current densities higher than ~125 $mA{\cdot}cm^{-2}$ at 650 °C, Fig. 7e. Although approximately similar effects of current density on the electrode performance were obtained under anodic polarization in air (Fig. 7 b, d and f), the area-specific resistance is lower under anodic in comparison to cathodic bias, with this difference greater with higher current, confirming the better electrode performance for the oxygen evolution reaction (OER) in comparison to the oxygen reduction reaction (ORR). Although $SrFe_{0.45}Co_{0.45}Mo_{0.1}O_{3-\delta}$ also performs better under anodic polarization, the effect is less apparent and only becomes significant in the higher range of currents at lower temperatures.

As mentioned above, the electrochemical process involving gaseous O_2 and the mixed-conducting oxide comprises the surface-exchange process from O_2 to oxide ions and the bulk diffusion of oxide ions in the bulk [30,31]. In this regard, Merkle et al. [30] noted that oxygen vacancies play the dominant role in bulk diffusion, but also in the surface-exchange process for "electron-rich" materials (including p-type electronic conductors) since the surface reaction involves not only an electron transfer but also an ion-site exchange. Furthermore, it was confirmed that the oxygen-migration energy is governed by the strength of the oxygen-cation bonds, which, in turn, is reported to play the dominant role in the electrochemical performance of perovskite-based cathodes [28]. The relative weakness of the Co–O bonds thus promotes higher oxide-ionic conductivity and the better electrochemical performance associated with the oxygen electrochemical kinetics observed in the present study.

Although oxygen vacancies at the surface play a key role in oxygen incorporation, a high diffusivity of vacancies in the bulk is also required for facilitating filling of the oxygen-vacancy site at the surface [32]. It follows, therefore, that the current density should impact the electrochemical performance, as it plays a role in accumulating or removing oxygen vacancies at the reaction sites.

The electrochemical performance under external dc polarization in air has previously been analysed for several electrode compositions such as LSM-based materials [33–35], $Ln_{n+1}Ni_nO_{3n+1}$ [24,36], $Ca_3Co_4O_9$ [37], $SrCo_{0.9}Ta_{0.1}O_{3-\delta}$ [38] $La_{0.3}Sr_{0.7}Fe_{0.7}Cr_{0.3}O_{3-\delta}$ [39], $SrCo_{0.9}Mo_{0.1}O_{3-\delta}$ [7] and even in metallic-Pt electrodes [24].

The manner in which the nature of the electrode material and the corresponding electrical transport properties affect the polarization behaviour of $La_{n+1}Ni_nO_{3n+1}$-based compositions was previously analysed in detail by Pérez-Coll et al. [24]. Current density was reported to have a strong influence on the electrochemical performance of $La_2NiO_{4+\delta}$ and $La_3Ni_2O_{7+\delta}$ electrodes, attributable to modification of the oxygen vacancies at reaction sites. It was also confirmed that improvement of the ionic conductivity of the cathode on addition of $Ce_{0.8}Sm_{0.2}O_{2-\delta}$ to form a composite considerably improved the ASR without a dc bias but, interestingly, the electrode process was less affected by the dc current density. It may be the case that, as oxide-ion diffusion becomes faster, the concentration of oxygen vacancies at active reaction sites is less affected by the current density. This hypothesis is supported by the low current-dependence of ASR observed in materials with high oxide-ionic conductivity, such as $SrCo_{0.9}Ta_{0.1}O_{3-\delta}$ [38], $SrCo_{0.9}Mo_{0.1}O_{3-\delta}$ [7], and the materials studied in the present work.

In this regard, Küngas et al. [40] studied the effect of current density on the electrochemical performance of LSF-YSZ composites and found an improvement in the low-frequency process of impedance spectra at higher currents for composites sintered at higher temperature. The authors concluded that this effect was associated with the oxygen adsorption rate at the surface, since dc polarization affects the oxygen-vacancy concentration. Modification of the microstructural properties of the composites, by sintering at lower temperature, led to practically invariant ASRs with current density, as expected for materials with a high oxide-ion diffusivity.

Fig. 8 shows the electrode overpotential for the title compositions as a function of the cathodic and anodic dc polarization. Notably, the studied compositions present lower overpotential curves under anodic bias. A similar improvement has previously been observed in several air-electrode materials with different mixed-conduction properties, such as La_2NiO_4 [24], $La_{0.3}Sr_{0.7}Fe_{0.7}Cr_{0.3}O_{3-\delta}$ [39], $SrCo_{0.9}Mo_{0.1}O_{3-\delta}$ [7] and $SrCo_{0.9}Ta_{0.1}O_{3-\delta}$ [38]. Under cathodic polarization, it is expected that both oxygen transport and oxygen adsorption limit the reduction reaction. However, under anodic polarization, bulk diffusion should be the principal influence in the electrochemical process, given that neither electron transfer in the oxygen evolution reaction nor desorption from the surface are expected to be rate limiting [41]. This conclusion highlights both the potential use of many SOFC cathode materials as prospective anodes in SOEC and of the feasibility of reversible SOFC-SOEC systems.

4. Conclusions

The substitution of Fe for Mo or Mo/Co in the cationic network of the oxygen-ordered $SrFeO_{3-\delta}$ perovskite stabilises the cubic phase at room temperature for compositions $SrFe_{0.9}Mo_{0.1}O_{3-\delta}$ and $SrFe_{0.45}Co_{0.45}Mo_{0.1}O_{3-\delta}$ and considerably improves electron-hole conductivity. The significant mass loss which occurs for all studied compositions at

temperatures higher than ~400–450 °C decreases the electronic conductivity and increases oxide ionic conductivity as temperature rises, as confirmed by Faradaic efficiency measurements of transport number. The lower bond strength of Co–O is reflected in a higher mobility of both electron holes and oxide ions, in addition to causing a higher thermal expansion coefficient for the Co-doped composition. The electrochemical behaviour is affected not only by the concentration of oxygen vacancies at reaction sites but also by oxide-ion diffusion through the bulk of the mixed-conducting phases. Although the polarization resistance is significantly lower for the Co-doped compound under conditions of no bias, the differences in performance between the studied phases diminish under dc bias at higher current densities in the intermediate temperature range. Slightly lower polarization resistances are obtained under anodic in comparison to cathodic bias. However, the excellent performance in both modes indicates the considerable potential of the studied system as air electrodes for reversible solid oxide fuel cell-electrolyser devices. In particular, the combination of lower thermal expansion, high electronic and ionic conductivity and low electrode polarization resistance under operating conditions offered by $SrFe_{0.9}Mo_{0.1}O_{3-\delta}$ renders this phase a highly promising reversible electrode.

Acknowledgements

The authors acknowledge the Fundación Domingo Martínez for financial support ("Ayuda a la investigación 2017. Área de Materiales: celdas de combustible"). We also thank the "Red de Excelencia" (MINECO, MAT2017-090695-REDT) for facilitating collaboration between the groups. We thank Dr. M.J. Pascual (ICV–CSIC) for supplying the glass-ceramic seal.

References

[1] C.-J. Winter, Hydrogen energy — abundant, efficient, clean: a debate over the energy-system-of-change, Int. J. Hydrogen Energy 34 (2009) S1–S52, https://doi.org/10.1016/j.ijhydene.2009.05.063.
[2] E. Wachsman, T. Ishihara, J. Kilner, Low-temperature solid-oxide fuel cells, MRS Bull. 39 (2014) 773–779, https://doi.org/10.1557/mrs.2014.192.
[3] A. Hauch, S.D. Ebbesen, S.H. Jensen, M. Mogensen, Highly efficient high temperature electrolysis, J. Mater. Chem. 18 (2008) 2331, https://doi.org/10.1039/b718822f.
[4] M.A. Laguna-Bercero, Recent advances in high temperature electrolysis using solid oxide fuel cells: a review, J. Power Sources 203 (2012) 4–16, https://doi.org/10.1016/j.jpowsour.2011.12.019.
[5] A.M. Svensson, S. Sunde, K. Nisancioglu, Mathematical modeling of oxygen exchange and transport in air-perovskite-yttria-stabilized zirconia interface regions, J. Electrochem. Soc. 145 (1998) 1390–1400, https://doi.org/10.1149/1.1838471.
[6] J.R. Mawdsley, J. David Carter, A. Jeremy Kropf, B. Yildiz, V.A. Maroni, Post-test evaluation of oxygen electrodes from solid oxide electrolysis stacks, Int. J. Hydrogen Energy 34 (2009) 4198–4207, https://doi.org/10.1016/j.ijhydene.2008.07.061.
[7] A. Aguadero, D. Pérez-Coll, J.A. Alonso, S.J. Skinner, J. Kilner, A new family of Mo-doped $SrCoO_{3-\delta}$ perovskites for application in reversible solid state electrochemical cells, Chem. Mater. 24 (2012) 2655–2663, https://doi.org/10.1021/cm300255r.
[8] Z.Q. Deng, W.S. Yang, W. Liu, C.S. Chen, Relationship between transport properties and phase transformations in mixed-conducting oxides, J. Solid State Chem. 179 (2006) 362–369, https://doi.org/10.1016/j.jssc.2005.10.027.
[9] J. Rodriguez, J.M. Gonzalez-Calbet, J.C. Grenier, J. Pannetier, M. Anne, Phase transitions in $Sr_2Co_2O_5$: a neutron thermodiffractometry study, Solid State Commun. 62 (1987) 231–234, https://doi.org/10.1016/0038-1098(87)90801-5.
[10] Q. Liu, X. Dong, G. Xiao, F. Zhao, F. Chen, A novel electrode material for symmetrical SOFCs, Adv. Mater. 22 (2010) 5478–5482, https://doi.org/10.1002/adma.201001044.
[11] L. Dos Santos-Gómez, J.M. Porras-Vázquez, E.R. Losilla, D. Marrero-López, Ti-doped $SrFeO_3$ nanostructured electrodes for symmetric solid oxide fuel cells, RSC Adv. 5 (2015) 107889–107895, https://doi.org/10.1039/c5ra23771h.
[12] L. Dos Santos-Gómez, J.M. Compana, S. Bruque, E.R. Losilla, D. Marrero-López, Symmetric electrodes for solid oxide fuel cells based on Zr-doped $SrFeO_{3-\delta}$, J. Power Sources 279 (2015) 419–427, https://doi.org/10.1016/j.jpowsour.2015.01.043.
[13] J.P. Hodges, S. Short, J.D. Jorgensen, X. Xiong, B. Dabrowski, S.M. Mini, C. W. Kimball, Evolution of oxygen-vacancy ordered crystal structures in the perovskite series $Sr_{(n)}Fe_{(n)}O_{(3n-1)}$ (n = 2, 4, 8, and ∞), and the relationship to electronic and magnetic properties, J. Solid State Chem. 151 (2000) 190–209, https://doi.org/10.1006/jssc.1999.8640.
[14] J.C. Waerenborgh, D.P. Rojas, a. L. Shaula, G.C. Mather, M.V. Patrakeev, V. V. Kharton, J.R. Frade, Phase formation and iron oxidation states in $SrFe(Al)O_{3-\delta}$ perovskites, Mater. Lett. 59 (2005) 1644–1648, https://doi.org/10.1016/j.matlet.2005.01.033.
[15] A. Aguadero, D. Pérez-Coll, C. de la Calle, J.A. Alonso, M.J. Escudero, L. Daza, $SrCo_{1-x}Sb_xO_{3-\delta}$ perovskite oxides as cathode materials in solid oxide fuel cells, J. Power Sources 192 (2009) 132–137, https://doi.org/10.1016/j.jpowsour.2008.12.138.
[16] W. Zhou, Z. Shao, R. Ran, R. Cai, Novel $SrSc_{0.2}Co_{0.8}O_{3-\delta}$ as a cathode material for low temperature solid-oxide fuel cell, Electrochem. Commun. 10 (2008) 1647–1651, https://doi.org/10.1016/j.elecom.2008.08.033.
[17] G. Xiao, Q. Liu, S. Wang, V.G. Komvokis, M.D. Amiridis, A. Heyden, S. Ma, F. Chen, Synthesis and characterization of Mo-doped $SrFeO_{3-\delta}$ as cathode materials for solid oxide fuel cells, J. Power Sources 202 (2012) 63–69, https://doi.org/10.1016/j.jpowsour.2011.11.021.
[18] R. Martínez-Coronado, J.A. Alonso, M.T. Fernández-Díaz, $SrMo_{0.9}Co_{0.1}O_{3-\delta}$: a potential anode for intermediate-temperature solid-oxide fuel cells (IT-SOFC), J. Power Sources 258 (2014) 76–82, https://doi.org/10.1016/j.jpowsour.2014.02.031.
[19] M.P. Pechini, Method of Preparing Lead and Alkaline Earth Titanates and Niobates and Coating Method Using the Same to Form a Capacitor, US Pat. No. 3330697, 1967. (n.d.).
[20] J. Rodríguez-Carvajal, Recent advances in magnetic structure determination by neutron powder diffraction, Phys. B Condens. Matter 192 (1993) 55–69, https://doi.org/10.1016/0921-4526(93)90108-I.
[21] M. Yuste, J.C. Pérez-Flores, J.R. de Paz, M.T. Azcondo, F. García-Alvarado, U. Amador, New perovskite materials of the $La_{2-x}Sr_xCoTiO_6$ series, Dalton Trans. 40 (2011) 7908, https://doi.org/10.1039/c1dt10196j.
[22] V. Kharton, A. Kovalevsky, A. Viskup, F. Figueiredo, J. Frade, A. Yaremchenko, E. Naumovich, Faradaic efficiency and oxygen permeability of $Sr_{0.97}Ti_{0.60}Fe_{0.40}O_{3-\delta}$ perovskite, Solid State Ion. 128 (2000) 117–130, https://doi.org/10.1016/S0167-2738(00)00275-7.
[23] D. Pérez-Coll, A. Aguadero, M.J. Escudero, P. Núñez, L. Daza, Optimization of the interface polarization of the La_2NiO_4-based cathode working with the $Ce_{1-x}Sm_xO_{2-\delta}$ electrolyte system, J. Power Sources 178 (2008) 151–162, https://doi.org/10.1016/j.jpowsour.2007.12.030.
[24] D. Pérez-Coll, A. Aguadero, M.J. Escudero, L. Daza, Effect of DC current polarization on the electrochemical behaviour of $La_2NiO_{4+\delta}$ and $La_3Ni_2O_{7+\delta}$-based systems, J. Power Sources 192 (2009) 2–13, https://doi.org/10.1016/j.jpowsour.2008.10.073.
[25] Y. Zhu, J. Sunarso, W. Zhou, S. Jiang, Z. Shao, High-performance $SrNb_{0.1}Co_{0.9-x}Fe_xO_{3-\delta}$ perovskite cathodes for low-temperature solid oxide fuel cells, J. Mater. Chem. A. 2 (2014) 15454, https://doi.org/10.1039/C4TA03208J.
[26] A.A. Markov, I.A. Leonidov, M.V. Patrakeev, V.L. Kozhevnikov, O.A. Savinskaya, U. V. Ancharova, A.P. Nemudry, Structural stability and electrical transport in $SrFe_{1-x}Mo_xO_{3-\delta}$, Solid State Ion. 179 (2008) 1050–1053, https://doi.org/10.1016/j.ssi.2008.01.026.
[27] Z. Deng, G. Zhang, W. Liu, D. Peng, C. Chen, Phase composition, oxidation state and electrical conductivity of $SrFe_{1.5-x}Co_xO_y$, Solid State Ion. 152–153 (2002) 735–739, https://doi.org/10.1016/S0167-2738(02)00317-X.
[28] T.T. Mayeshiba, D.D. Morgan, Factors controlling oxygen migration barriers in perovskites, Solid State Ion. 296 (2016) 71–77, https://doi.org/10.1016/J.SSI.2016.09.007.
[29] R. Merkle, J. Maier, How is oxygen incorporated into oxides? A comprehensive kinetic study of a simple solid-state reaction with $SrTiO_3$ as a model material, Angew. Chem. Int. Ed. 47 (2008) 3874–3894, https://doi.org/10.1002/anie.200700987.
[30] R. Merkle, J. Maier, H.J.M. Bouwmeester, A linear free energy relationship for gas-solid interactions: correlation between surface rate constant and diffusion coefficient of oxygen tracer exchange for electron-rich perovskites, Angew. Chem. Int. Ed. 43 (2004) 5069–5073, https://doi.org/10.1002/anie.200460081.
[31] N.H. Perry, T. Ishihara, Roles of bulk and surface chemistry in the oxygen exchange kinetics and related properties of mixed conducting perovskite oxide electrodes, Materials 9 (2016) 858, https://doi.org/10.3390/ma9100858.
[32] Y. Chen, W. Zhou, D. Ding, M. Liu, F. Ciucci, M. Tade, Z. Shao, Advances in cathode materials for solid oxide fuel cells: complex oxides without alkaline earth metal elements, Adv. Energy Mater. 5 (2015) 1500537, https://doi.org/10.1002/aenm.201500537.
[33] S.P. Jiang, J.G. Love, J.P. Zhang, M. Hoang, Y. Ramprakash, A.E. Hughes, The electrochemical performance of LSM/zirconia – yttria interface as a function of a-site non-stoichiometry and cathodic current treatment, Solid State Ion. 121 (1999) 1–10.
[34] X.J. Chen, K.A. Khor, S.H. Chan, Electrochemical behavior of $La(Sr)MnO_3$ electrode under cathodic and anodic polarization, Solid State Ion. 167 (2004) 379–387, https://doi.org/10.1016/j.ssi.2003.08.049.
[35] S. McIntosh, S.B. Adler, J.M. Vohs, R.J. Gorte, Effect of polarization on and implications for characterization of LSM-YSZ composite cathodes, Electrochem. Solid State Lett. 7 (2004). A111–A114.
[36] F. Mauvy, C. Lalanne, J.-M. Bassat, J.-C. Grenier, H. Zhao, L. Huo, P. Stevens, Electrode properties of $Ln_2NiO_{4+\delta}$ (Ln= La, Nd, Pr) AC impedance and DC polarization studies, J. Electrochem. Soc. 153 (2006), https://doi.org/10.1149/1.2207059. A1547–A1553.
[37] J.R.D. Santos, F.J.A. Loureiro, J.P.F. Grilo, V.D. Silva, T.A. Simões, D.P. Fagg, D. A. Macedo, Understanding the cathodic polarisation behaviour of the misfit $[Ca_2CoO_{3-\delta}]_q[CoO_2]$ (C349) as oxygen electrode for IT-SOFC, Electrochim. Acta 285 (2018) 214–220, https://doi.org/10.1016/J.ELECTACTA.2018.08.018.

[38] J. Wang, T. Yang, L. Lei, K. Huang, Ta-Doped $SrCoO_{3-\delta}$ as a promising bifunctional oxygen electrode for reversible solid oxide fuel cells: a focused study on stability, J. Mater. Chem. A. 5 (2017) 8989–9002, https://doi.org/10.1039/C7TA02003A.

[39] B. Molero-Sánchez, P. Addo, A. Buyukaksoy, S. Paulson, V. Birss, Electrochemistry of $La_{0.3}Sr_{0.7}Fe_{0.7}Cr_{0.3}O_{3-\delta}$ as an oxygen and fuel electrode for RSOFCs, Faraday Discuss 182 (2015) 159–175, https://doi.org/10.1039/C5FD00029G.

[40] R. Küngas, A.S. Yu, J. Levine, J.M. Vohs, R.J. Gorte, An investigation of oxygen reduction kinetics in LSF electrodes, J. Electrochem. Soc. 160 (2013), https://doi.org/10.1149/2.011303jes. F205–F211.

[41] A. Barbucci, P. Carpanese, G. Cerisola, M. Viviani, Electrochemical investigation of mixed ionic/electronic cathodes for SOFCs, Solid State Ion. 176 (2005) 1753–1758, https://doi.org/10.1016/j.ssi.2005.04.027.